JOURNAL OF PLANKTON RESEARCH | VOLUME 32 | NUMBER 5 | PAGES 585–601 | 2010

A broad spatio-temporal view of the Western English Channel observatory

TIMOTHY J. SMYTH*, JAMES R. FISHWICK, LISA AL-MOOSAWI, DENISE G. CUMMINGS, CAROLYN HARRIS, VASILLIS KITIDIS, ANDREW REES, VICTOR MARTINEZ-VICENTE AND ERNEST M. S. WOODWARD

PLYMOUTH MARINE LABORATORY, PROSPECT PLACE, PLYMOUTH, DEVON PL1 3DH, UK

*CORRESPONDING AUTHOR: tjsm@pml.ac.uk

Received March 17, 2009; accepted in principle October 23, 2009; accepted for publication November 29, 2009

Corresponding editor: Roger Harris

The marine laboratories in Plymouth have sampled at two principle sites in the Western English Channel for over a century in open-shelf (station E1; 50° 02′N, 4° 22′W) and coastal (station L4; 50° 15′N, 4° 13′W) waters. These stations are seasonally stratified from late-April until September, and the variable biological response is regulated by subtle variations in temperature, light, nutrients and meteorology. Station L4 is characterized by summer nutrient depletion, although intense summer precipitation, increasing riverine input to the system, results in pulses of increased nitrate concentration and surface freshening. The winter nutrient concentrations at E1 are consistent with an open-shelf site. Both stations have a spring and autumn phytoplankton bloom; at station E1, the autumn bloom tends to dominate in terms of chlorophyll concentration. The last two decades have seen a warming of around 0.6°C per decade, and this is superimposed on several periods of warming and cooling over the past century. In general, over the Western English Channel domain, the end of the 20th century was around 0.5°C warmer than the first half of the century. The warming magnitude and trend is consistent with other stations across the north-west European Shelf and occurred during a period of reduced wind stress and increased levels of insolation (+20%); these are both correlated with the larger scale climatic forcing of the North Atlantic Oscillation.

INTRODUCTION

Since the 1980s, the rate of sea surface temperature (SST) rise around the UK has been about 0.2–0.6°C per decade (MCCIP, 2008) and this warming has been fastest in the English Channel and southern North Sea. Climate models indicate a continuation of this rise with the most pronounced warming predicted for the Celtic, Irish and southern North Seas. Stratification strength is also predicted to increase but substantially less so on the continental shelf compared with the deep seas (UKCP09, 2009). The biological response to these changes, such as the migration of particular marine organisms (Beaugrand and Reid, 2003; Zacherl *et al.*, 2003; Beaugrand, 2004; Hawkins *et al.*, 2008; Hiddink and ter Hofstede, 2008; Beaugrand *et al.*, 2009) and changes in the timing of the spring phytoplankton bloom (Wiltshire and Manly, 2004; Sharples *et al.*, 2006; Nicklisch *et al.*, 2008; Sommer and Lengfellner, 2008; Vargas *et al.*, 2009), have all been studied. It is therefore important that continuous monitoring programs, such as the Western Channel Observatory (WCO), are established and maintained in these complex shelf regions, to quantify and validate these predicted changes.

The WCO is situated in the Western English Channel and comprises of several long-term sustained observations, principally at stations L4 (50° 15′N, 4° 13′W; depth 50 m) and E1 (50° 02′N, 4° 22′W; depth 75 m). These stations have a long history of *in situ* sampling

doi:10.1093/plankt/fbp128, available online at www.plankt.oxfordjournals.org. Advance Access publication December 27, 2009

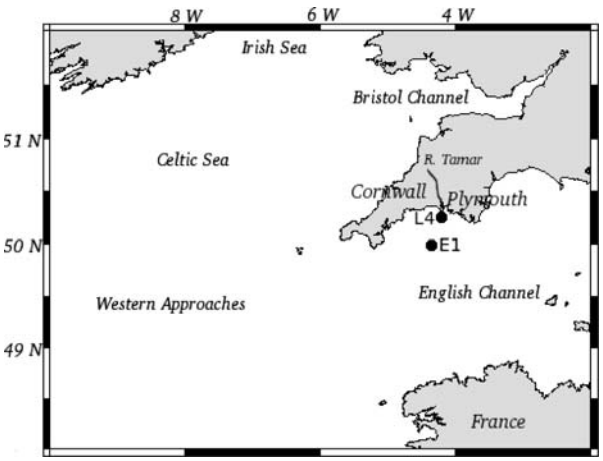

Fig. 1. Map showing the locations of L4 and E1 within the wider context of the WCO domain.

(Southward *et al.*, 2005) and represent both open shelf (E1) and coastal waters (L4) within 40 km of Plymouth (Fig. 1) allowing frequent sampling, weather permitting, throughout the year. The Western English Channel is ideal for detecting ecosystem responses to climate change, including interactions with large-scale impacts such as fishing (Araujo *et al.*, 2006), without the confounding effect of more localized and regional impacts (e.g. eutrophication). The region straddles biogeographical provinces with both boreal/cold temperate and warm temperate species present (Southward *et al.*, 2005), giving early warning of change in species composition and distribution elsewhere.

L4 has been sampled continuously by the Plymouth Marine Laboratory since 1988 with an initial emphasis on zooplankton measurements. E1 represents the long-term hydrographical series originally started in 1903 by the Marine Biological Association (MBA), which is unbroken apart from the hiatus caused by the World Wars and organizational changes in the late 1980s and 1990s. E1 may be described as an open-shelf station, well away from coastal freshwater influences but not fully oceanic as the shelf break, some 350 km to the south-west, forms an efficient barrier to transfers of water between the shelf and the open Atlantic. However, when compared with other long-term stations situated in the Irish and North Seas, E1 is subject to higher salinities and lower phosphate concentrations, and has been assumed (Laane *et al.*, 1996) to be representative of the natural signal of Atlantic water entering the shelf seas.

The hydrography at E1 is characterized by the development of a seasonal thermocline: typically stratification starts in May, persists throughout the summer and is eroded by the end of October. The typical depth of the summer thermocline is around 20 m. Station L4 is periodically affected by riverine inputs of the Tamar estuary and the magnitude of these is determined by recent rainfall, wind mixing and the state of the tide. L4 is also seasonally stratified throughout the summer period. Both stations are tidally influenced (0.6 ms^{-1} maximum surface stream at mean spring tide) with a predominantly sandy sea bed (Pingree, 1980). As to be expected, both stations are strongly affected by ambient weather conditions.

This paper examines the wider spatio-temporal context within which the WCO is situated. The spatial dimension is studied using satellite remote sensing of sea-surface temperature (SST) and ocean colour. The temporal is examined in terms of the fundamental ecosystem determinants of temperature, salinity, light, nutrients, chlorophyll and meteorology. These are analysed in terms of seasonality and for trends in the individual time-series.

METHOD

Remote sensing

Monthly SST climatologies for the period 1985–2001 were obtained from version 5.0 of the AVHRR Pathfinder (Pathfinder, 2009) data set. (This is the latest climatological period available.) These global data were at 4 km resolution and night-time climatologies were used to avoid the problems of diurnal heating (Schluessel *et al.*, 1990). Data were extracted for the region 48–52°N, 10–2°W and the monthly mean images smoothed using a boxcar average over a 16 pixel wide moving window to achieve smooth contouring. Unsmoothed data from the entire Pathfinder data set (1985–2007) was used for the point satellite data extractions at L4 and E1, and a time-series of monthly anomalies constructed. Monthly chlorophyll-*a* (O'Reilly *et al.*, 1998) climatologies (V5.2) from the Sea-viewing Wide-Field-of-view Sensor (SeaWiFS) were obtained from the OceanColor Web (OceanColorWeb, 2009) for the period 1998–2007. As for SST, the data were extracted for the region of interest and smoothed.

Meteorological parameters

Surface meteorological parameters for the grid point closest to the location of L4 and E1 (50°N, 4°W) were obtained from the European Centre for Medium Range Weather Forecasting (ECMWF) ERA-40 data set for the period between 1958 and 2007. The parameters extracted were the vector wind (split into zonal and meridional components) and percentage cloud cover. The daily wind data were then averaged over each calendar month of the time-series.

Monthly averaged North Atlantic Oscillation (NAO, 2009) data were also obtained for the same period, so the larger scale forcing could be related to the local scale effects. For an historical comparison (Southward *et al.*, 1975), sunspot data were also obtained (NOAA, 2009).

Incident irradiance

Incident irradiance was calculated using the Gregg and Carder (Gregg and Carder, 1990) spectral model for cloudless marine atmospheres, rather than relying upon sporadic *in situ* solar irradiance data. This was modified for clouds, taken from the ECMWF ERA-40 analyses, using the formulation of Reed (Reed, 1977). The model was run using a standard atmosphere (surface pressure 1013 mb; relative humidity 75%; visibility 15 km; aerosol angstrom exponent 0.8; perceptible water 2 cm; ozone concentration 270 DU) for the nominal location in the Western English Channel (50°N, 4°W). The model was run at 5 nm wavelength resolution between 400 and 700 nm with a time step of 30 min and integrated over time and wavelength to obtain total daily PAR (mol photons m^{-2} day^{-1}) for each day of the year between 1958 and 2007. The daily data were then further averaged to give a monthly mean irradiance covering the time-series. Finally, a climatological mean monthly PAR was determined and the percentage anomaly for each individual month from this climatological mean calculated.

In situ temperature and salinity

Early in the time-series (1903–1987), temperature and salinity depth profiles were determined using reversing mercury thermometers and salinity bottles at E1; surface measurements also being taken using a scientific bucket and thermometer. In the electronic era instruments changed between two different systems: 1988–2001 used a CTD developed at PML (Aiken, 1984); post 2002 used a SeaBird SBE19+. At L4, surface temperatures were measured using a thermometer and bucket 1988–1998, PML CTD system 1998–2002 and SeaBird SBE19+ post 2002. There are obvious drawbacks to not having consistent instrumentation throughout a time-series (Parker *et al.*, 1995), especially as there was insufficient overlap to carry out a rigorous difference analysis. It is also difficult to carry out a proper error analysis of the different component data sets. For example, surface-collected bucket samples are subject to convective heating by direct insolation and conduction, depending on the bucket material, when on the deck. The frequency of calibration is not known for the mercury thermometers. Without these sources of metadata and a full description of the instrumentation used, it is difficult to properly quantify the errors. However, it is likely that the older parts of the data set are subject to larger errors than more recent data. Using this as a rule of thumb, qualitative errors can be arrived at. For the temperature data set, a realistic error is $\pm 0.1^{\circ}$C for the bucket and mercury in glass thermometers, whereas the SeaBird SBE19+ has a likely accuracy of $\pm 0.001^{\circ}$C. The same qualitative error analysis can be applied to the salinity data set with an accuracy of ± 0.05 (using salinity standards) early in the data set and ± 0.01 for the recent electronic data. The accuracy of the salinity values since 2002 has been periodically verified by simultaneously measuring with two or more SBE19+ units through the water column.

To cover the hiatus in the time-series between 1987 and 2002, especially marked for E1, point data extractions from the monthly AVHRR Pathfinder data set were used. For consistency, all data types were used to calculate the climatological monthly mean temperature; the individual monthly anomalies were then determined as a simple difference from this. The quoted global accuracy of the Pathfinder data set is $0.14 \pm 0.36^{\circ}$C.

Heat budget

A simple heat budget was calculated for the E1 site using the *in situ* measurements of SST (satellite data were used to replace missing data) and ECMWF ERA-40 meteorological parameters of surface wind, air temperature, humidity and cloud cover data. The budget can be described thus:

$$Q_T = Q_{SW} + Q_{LW} + Q_S + Q_L + Q_V \quad (\mathrm{Wm}^{-2}) \qquad (1)$$

where Q_T is the total heat flux into the ocean; Q_{SW} the solar (short wave) input; Q_{LW} the heat lost by long wave radiation; Q_S the sensible heat flux; Q_L the latent heat flux and Q_V the advection term (which was neglected). The Matlab® codes used to carry out this analysis were downloaded from the Woods Hole Science Center web site (WHSC, 2009). Essentially, Q_{SW} is a function of cloud-cover, latitude and time of year; Q_{LW} a function of cloud-cover, sea and air temperature and humidity; Q_S is a function of wind speed, sea and air temperature and Q_L a function of wind speed and humidity. Equation (1) was used to calculate a heat budget on a daily basis between 1957 and 2007 and the E1 SSTs were interpolated from a coarse monthly grid onto a daily grid using linear interpolation. A monthly mean was then calculated, and a departure from that monthly mean (anomaly) for each data point constructed. Finally, the data were put through a running 5-year median filter so the net heat flux anomaly could be calculated.

Nutrients

Surface measurements of the major nutrient species were taken weekly at L4 and depth profiles monthly at E1. After 2004, analysis was carried out using fresh (rather than frozen) samples to overcome possible sampling and storage artefact issues. All nutrient concentrations were determined using recognized analytical techniques (Woodward and Rees, 2002) as follows: phosphate (Zhang and Chi, 2002), silicate (Kirkwood, 1989), nitrate and nitrite ions (Brewer and Riley, 1965), and nitrite analysis (Grasshoff, 1976). Nitrate concentrations were calculated by subtracting the nitrite from the combined nitrate plus nitrite concentration.

Chlorophyll *a*

One or 2 L of seawater was filtered onto a Whatman® GF/F glass microfibre filter and the filter stored in liquid nitrogen until the analysis. For the analysis stage, pigments were extracted from the thawed GF/F filter into 2 mL methanol (Llewellyn *et al.*, 2005) and sonicated for 35 s. These extracts were then centrifuged to remove filter and cell debris (5 min at 4000 rpm) and analysed using reversed-phase HPLC (Barlow *et al.*, 1997). Pigments, including chlorophyll *a*, were identified using retention time and spectrally matched using photo-diode array spectroscopy (Jeffrey and Wright, 1997). Pigment concentrations were determined by response factors, generated at the time of instrument calibration, using a suite of pigment standards. For fluorometrically determined chlorophyll *a*, 0.1 L of seawater was filtered through GF/Fs in triplicate and the JGOFS (JGOFS, 1994) protocols adhered to.

HPLC chlorophyll-*a* data were only available between 1999 and 2008 from L4, whereas the fluorometrically determined values spanned a longer portion of the time-series between 1992 and 2008. Therefore, to give a longer time period of observations, both data sets were merged; HPLC being used in preference to fluorometric where available. The agreement between the HPLC and fluorometrically derived values was close with the following regression statistics: slope = 0.989, bias = 0.0026 and $r^2 = 0.98$.

RESULTS

Remote sensing: the wider picture

Figure 2 shows the seasonal transition between mixing and stratification. The winter months (December–March) are characterized by a latitudinal variation in temperature (warm in the south, cold in the north), this pattern only being interrupted by land boundaries. Starting around May, and lasting until September, an increasingly heterogeneous pattern emerges between the stratified Celtic Sea and Western approaches and regions subject to strong tidal mixing. Notable regions include the southern Irish Sea, the Penwith Peninsula (in the west of Cornwall), Ushant (north-western France), the Bristol Channel and the mid-English Channel. These strong horizontal temperature gradients are the surface manifestation of tidal mixing fronts (Simpson, 1981) and are controlled by variations in the intensity of tidal stirring. These frontal regions have also been shown to be biologically important (Pingree *et al.*, 1975). The temperature gradients are most intense in July and August. The temperature gradient between the Celtic and southern Irish Sea is around 1°C every 10 km. The cooling effect of enhanced tidal mixing off Ushant and the Penwith Peninsula is around 2°C, although the effect may be stronger than this during spring tides (and weaker during neaps). The tidal stream amplitude at these two locations is 2–2.5 and 1–1.5 ms^{-1}, respectively (Pingree, 1980), which is above the background 0.5–1 ms^{-1} typical of the Western English Channel, and the bottom stress is of order 1–2 Nm^{-2}. A visual inspection of the differences between the 1905–1954 climatologies presented in Pingree (Pingree, 1980) shows that typically the 1985–2001 climatologies are around 0.5°C warmer right across the domain and the August climatology may be up to 1°C warmer. However, it must be noted that these two sets of climatologies were arrived at using different measurement techniques.

Figure 3 shows that the typical background chlorophyll concentration in the Western English Channel is around 1 mg m^{-3} throughout the year. Winter (October–March) is characterized by higher "chlorophyll" around the coast. However, these are likely artefacts caused by elevated values of suspended particulates and/or coloured dissolved organic matter which confounds the satellite chlorophyll algorithm (Sathyendranath *et al.*, 1989). The first sign of the spring bloom, consistent with an earlier onset of stratification (Pingree, 1980), is in April in the Celtic Sea with chlorophyll values between 1 and 3 mg m^{-3}. The values in the Western English Channel remain at 1 mg m^{-3} for this month. However, bloom conditions last longer in the Western English Channel with particularly elevated chlorophyll in the central Western English Channel from June, especially in July, and into August. This localized maximum marks the most common position of summer blooms of either *Karenia mikimotoi* (Pingree *et al.*, 1975) or *Emiliana huxleyi* (Smyth *et al.*, 2002); the latter being characterized by much lower chlorophyll concentrations than the former. During the

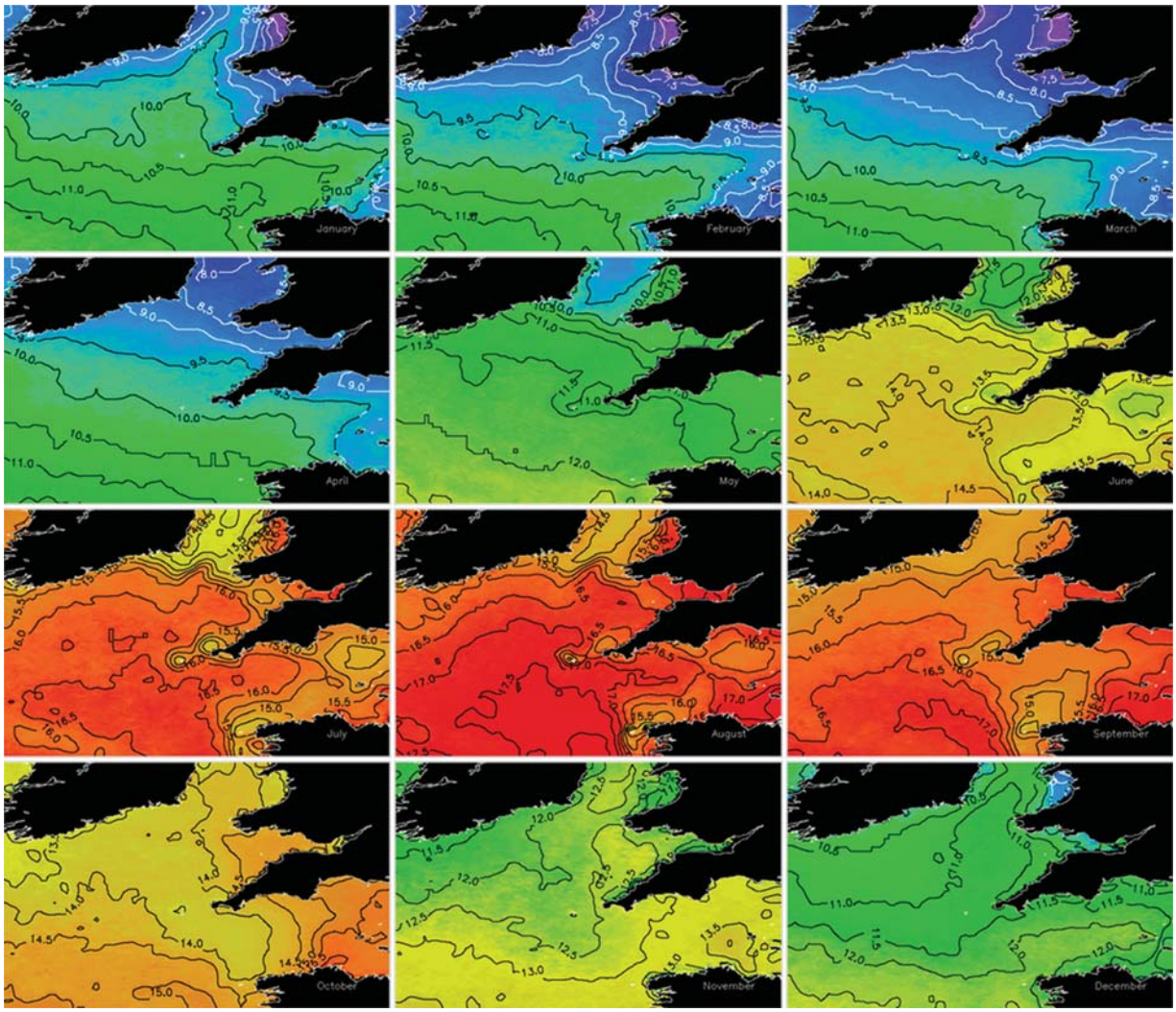

Fig. 2. Mean monthly SST climatologies (1985–2001), derived from the Pathfinder AVHRR time-series and contoured at 0.5°C intervals.

summer period, there is a pronounced reduction in phytoplankton towards the southwest of the domain, with some parts of the Western approaches having chlorophyll concentrations <0.3 mg m^{-3}. The chlorophyll increases with the approach of autumn with the breakdown in stratification and the mixing of nutrients into the surface layer. It should be noted here that Fig. 3 is a mean of 10 years' satellite derived chlorophyll *a* over an entire month. The averaging process has the effect of smearing out point events and lessening their impact. The absolute magnitude of the spring bloom for example in the Celtic Sea has been reported to be as high as 5.5 mg m^{-3} (Fasham *et al.*, 1983) and 8 mg m^{-3} (Pingree, 1980). Estimated chlorophyll from SeaWiFS during a central Western English Channel bloom of *Karenia mikimotoi* (corroborated by unpublished *in situ* data) in July 2000 was >60 mg m^{-3}.

Physical forcing

The 50-year time-series of modelled wind data, extracted from the ERA-40 analyses, shows a high degree of variability (Fig. 4), with the wind speed varying between 0 and 10 ms^{-1} (median around 3.0 ms^{-1} over the past decade). The dominant and strongest winds come from the south-west quadrant, with the least frequent winds coming from the north-east. Applying a 5-year running median filter to the zonal wind component (Fig. 4) shows a degree of decadal periodicity, with weaker westerly winds during the 1970s and in the 1990s. Also shown is the North Atlantic Oscillation (NAO, 2009) Index with an annual running median filter applied to the monthly averaged data. If an annual running median filter is applied to both the NAO and the zonal wind data, the correlation is 0.40 (incidentally, the correlation between sun spot cycle and zonal wind strength is 0.23, with a

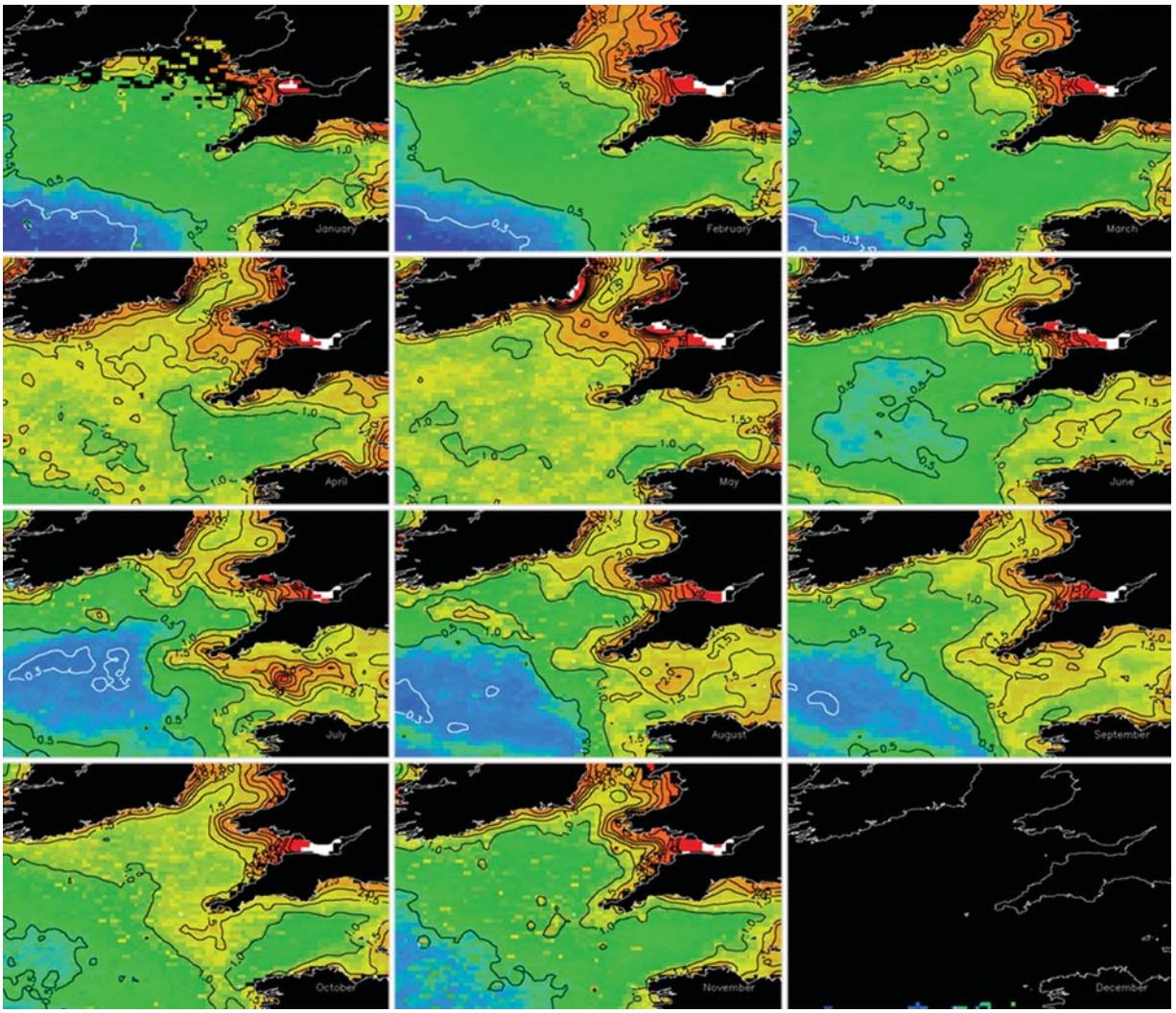

Fig. 3. Mean monthly chlorophyll climatologies (1998–2007), derived from the SeaWiFS ocean colour time-series and contoured at irregular intervals (0.3, 0.5, 1, 1.5, 2, 2.5, 3, 3.5, 4, 4.5, 5, 5.5, 6 mg m^{-3}). In December, the solar illumination is insufficient for the satellite remote sensing of ocean colour.

weaker correlation between sun spots and the NAO of 0.08). The meridional wind does not display the same periodicity, with the median southerly wind component being around 0.5 ms^{-1} and a weaker correlation (0.15) with the NAO.

The corresponding PAR anomaly 50-year time-series (Fig. 5) shows a high degree of variability on a month-by-month basis. The surface PAR can vary by almost 150% according to these modelled results. In reality, the PAR variability at the surface is likely to be more than this. The theoretical effect of adding clouds, from clear to completely overcast, is to reduce the daily insolation by a factor of two: in January the variation is between 3.5 and 7 mol photons m^{-2} day^{-1} and in July between 33 and 57 mol photons m^{-2} day^{-1}. However, the Reed's (Reed, 1977) cloud model is highly generalized and only uses a single (percentage) cloud cover for a 24-h period. There is no input information on the height or type of clouds: for instance, the radiant properties of cirrus are very different to nimbostratus. Over longer time-periods, it is likely that these short temporal variations become less important. Applying a 5-year running median filter to the PAR anomalies (Fig. 5) shows a degree of coherence, with the first 20 years of the time-series showing a long-term decrease in the amount of PAR received at the surface by around 20% and a corresponding increase over the last 20 years. There are signs that over the past 5 years, the trend has somewhat stabilized and is possibly starting to decline. When correlated to the larger scale forcing of the NAO, there is a negative correlation ($r = -0.20$), i.e. when the westerly (Atlantic) winds are weaker there is more

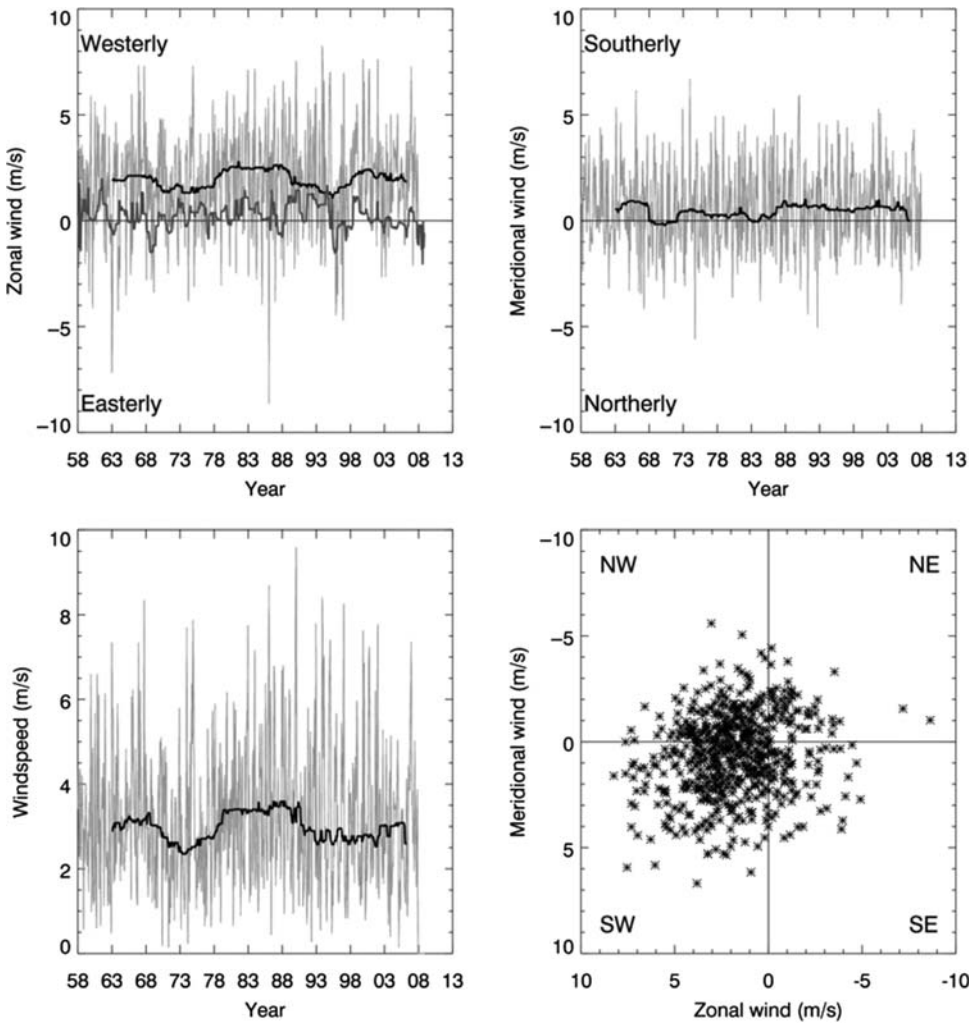

Fig. 4. Variations in the zonal (west–east), meridional (south–north) vector winds, the total windspeed and wind direction for the period 1958–2007. All wind data extracted for a grid point at 50°N, 4°W from the ECMWF ERA-40 midnight analyses and averaged over a calendar month. A 5-year running median is plotted as the solid black line with the monthly averaged NAO, filtered through a 12-month running median, overlaid as the lower solid dark grey line on the zonal wind plot.

incident PAR. This is most clearly seen in a direct comparison between the zonal wind strength (Fig. 4) and the PAR anomaly (Fig. 5). The period between 1978 and 1990 was characterized by stronger zonal (westerly) winds. This matches the negative PAR anomaly where there was a strong and sustained drop in PAR by around 10%. Although the NAO was not strongly positive during this period, it was dominated by positive (more westerly) values. The stronger westerly winds imply a dominance of Atlantic depressions bringing cloud (and hence the drop in PAR), wind and rain over the UK.

Temperature

The E1 sea-surface temperature time-series (Fig. 6) shows considerable temperature variability over the 20th century with surface monthly anomalies ranging between $\pm 2^{\circ}$C of the 1903–2007 long-term mean. There are several periods of warming and cooling: a warming in the 1920s and 1930s (Southward, 1960); a cooling in the 1940s and 1960s; a pronounced warming in the 1950s and a warming from the mid-1980s to the present. Currently, the surface temperatures are around 0.8°C above the long-term average, with the rapid temperature increase (+0.6°C per decade over the past 20 years: slope = 0.06; $r^2 = 0.21$) from the mid-1980s to the present, being captured by the satellite record.

Towards the bottom of the water column (50 m), the recent temperature anomalies are particularly notable and are of order 0.7°C above the long-term average. This implies that the warming is not limited to the surface and the whole water column is affected.

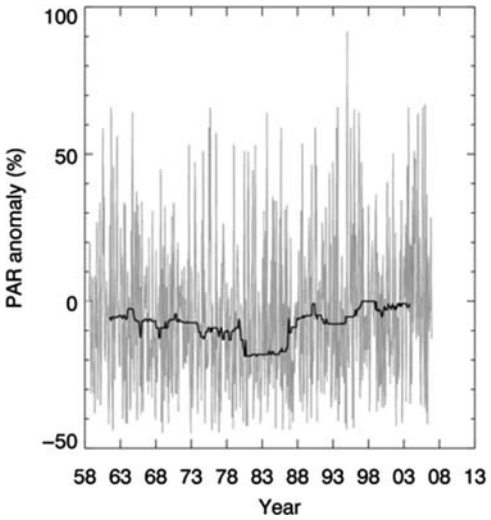

Fig. 5. Variations in the calculated (Gregg and Carder, 1990) monthly PAR anomaly for a grid point at 50°N, 4°W using cloud coverage data from the ECMWF ERA-40. A 5-year running median is plotted as the solid black line.

The mean monthly surface temperatures (Fig. 6) range from a minimum of 9.2°C in March, to a maximum of 16.5°C in August, with the 2σ envelope ranging between ± 0.7 and ± 1.3°C around the mean. The mean monthly 50 m temperature has a minimum of 9.1°C in March and a maximum (following the breakdown in stratification) of 14.1°C in October. The 2σ envelope has a smaller range than at the surface and is between ± 0.5 and ± 0.7°C around the mean at 50 m.

The surface and bottom temperatures were used to determine the onset date of thermal stratification, defined as a +0.1°C difference between the surface and bottom temperature. No appreciable trend was found over the entire centennial time-series, although the temporal coarseness of the sampling routine at E1 could be partially to blame as the station is only sampled once per month. The median date for the start of thermal stratification was found to be day 121 (1 May). This is in good agreement with previous dates arrived at (Pingree, 1980).

The heat balance anomaly analysis (Fig. 7) shows that for the period between 1963 and 1978, the net heat flux anomaly was around $+10$ W m^{-2} (i.e. into the sea). The following decade was characterized by a negative anomaly of -8 W m^{-2} (i.e. heat lost by the sea). The period between the mid-1980s and the late 1990s was characterized by a rapid reversal in this with a short-lived peak around 1998 of $+30$ W m^{-2}. This uptake of heat by the sea corresponds to the period of warming of 0.6°C per decade at E1. The correlation between wind speed (Fig. 4) and the net heat flux anomaly was -0.52. The correlation between the incoming solar radiation (represented by Fig. 5) and the net heat flux anomaly was 0.87. However, caution must be taken when analysing the correlation between the net heat flux and SST and net heat flux and the various meteorological parameters as these were the measurements used to force the model.

Figure 8 shows that the temperature anomaly time-series for L4 appears to be much noisier than for E1 (Fig. 6). However, this could be an artefact caused by more frequent sampling at L4 (weekly whereas E1 is typically monthly). The monthly averages are remarkably similar to E1: a surface minimum of 9.1°C in March and a maximum of 16.4°C in August with a similar envelope of variability. However, the averages were calculated over different time periods (1903–2007 for E1; 1988–2007 for L4). As the L4 time-series was calculated over a warmer phase, these similarities in the mean-monthly temperatures are misleading. Comparison between Figs 6 and 8 shows that L4 is cooler than E1 by approximately 0.5°C for the period January–June. In July, E1 is around 1°C warmer, but for the period September–November L4 is slightly warmer by between 0.1 and 0.3°C. Both stations show a warming over the period 1985–2007. The onset of stratification, as for station E1, has not changed appreciably over the 20-year time-series. Using a more conservative +0.5°C difference between the surface and 30 m, the median date for the onset of stratification is 23 April.

Figures 6 and 8 show a possible superposition of background climate effects and ambient meteorology by showing the temperature data for 2007 (asterisks). The summer period of 2007 was notable for being wet and overcast. This hampered the warming of the surface layers by insolation and the subsequent development of a strong thermocline. This limited the temperature throughout the water column (seen at both the surface and 50 m) to around the climatological average. However, both the winter/early spring and autumn periods, which are characterized by well mixed water columns at both L4 and E1, have temperatures that are the highest ever recorded in the respective series. This apparent paradox of limited summer surface warming being followed by warmer than average winter temperatures may be partially explained by the surface layer being relatively thin compared with the bottom waters. At L4, the surface layer is typically 10–15 m (cf. 50 m total water column). Also a warmer surface layer loses considerably more heat back to the atmosphere with the onset of autumn and so has a relatively slight impact on the final mixed temperature. It is likely that winter sea temperatures are more strongly related to winter air temperatures (Sharples *et al.*, 2006).

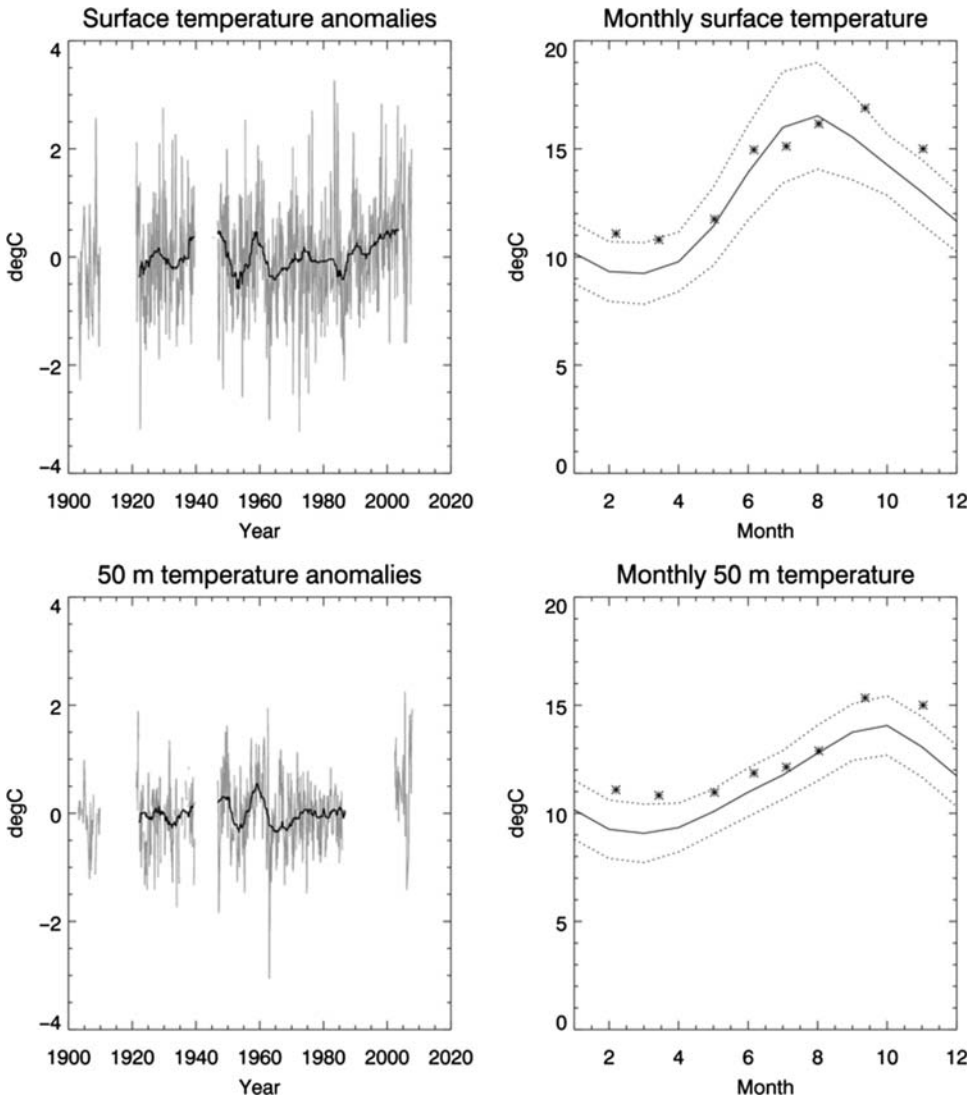

Fig. 6. E1 surface and 50 m temperature time-series analysis. Top panels show the temperature anomalies and monthly averaged temperature for the surface layer (around 2 m) and the corresponding 5-year running median. Bottom panels show the anomalies and averages at 50 m depth. Asterisks represent the data for 2007 and dashed lines the 2σ (2 standard deviations) around the mean during the series. The data between 1987 and 2002 in the upper left panel are monthly averaged satellite SSTs extracted from the Pathfinder data set.

Salinity

The waters at E1 (Fig. 9) are typically more saline than at L4 (Fig. 10) by around 0.1 (but again note the difference in the averaging time period). Station L4 clearly shows the localized effect of riverine inputs, with sharp, pulsed delta-functions of lower salinity, freshening the water by up to −1. These fresher pulses are not apparent at 50 m depth, which implies that these are surface lenses of fresher water from the River Tamar. Indeed individual salinity profiles (not shown here) at L4 frequently demonstrate the freshening to be restricted to the top 2–25 m of the water column depending on the severity of the event. Localized intense precipitation could also account for some of the surface freshening, but not for changes in sea-water chemistry which is episodically measured (Rees *et al.*, 2009). Also the magnitude of some of the freshening events observed discounts localized precipitation from being the sole cause. For example, February 2007 saw a freshening of 0.5 though the water column to a depth of 25 m. If all the freshening was solely due to local precipitation (i.e. neglecting the advection component), the amount of rainfall required would be in excess of 350 mm. Only 175 mm was recorded at the Plymouth Marine Laboratory meteorological station over the entire month.

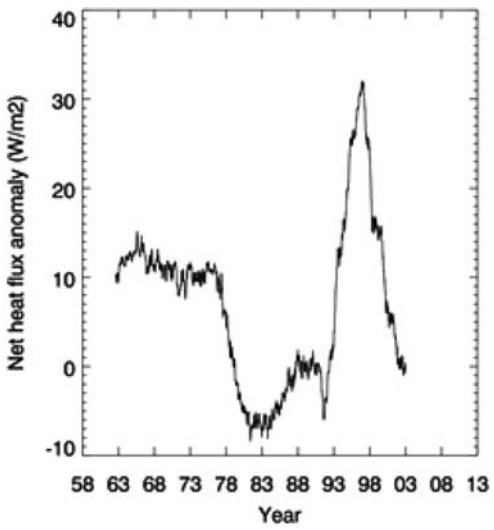

Fig. 7. E1 net head flux anomaly calculated using E1 SST data and daily meteorological parameters extracted from the ECMWF ERA-40 data set between 1957 and 2007. The data are plotted as anomalies from the mean monthly net heat flux and filtered using a 5-year running median.

Nutrients

The monthly averaged nitrate (Fig. 11) shows a variation of between 8 μM in January to below the detectable limit between May and July at L4. Similar values (asterisks) are observed at the shorter, coarser resolution time-series available from E1. The winter values are in good agreement with previous open shelf sea work; Hydes *et al.* (Hydes *et al.*, 2004) report a value of 7.4 μM on the Malin Shelf (area around 56° 30′N, 9°W) contrasting with 11 μM of nitrate in the north Atlantic oceanic waters. West of the Celtic Sea shelf break (area around 48° 45′N, 10° 30′W), Hydes *et al.* (Hydes *et al.*, 2004) reported nitrate values between 6.5 and 8.5 μM. The period of the spring bloom is characterized by a rapid depletion in nitrate as the phytoplankton grow (March–April). This, as Pingree *et al.* (Pingree *et al.*, 1977) observe, is before the thermocline becomes permanently established. The length of the spring bloom is constrained by the exhaustion of nitrate. The erosion of the thermocline and the breakdown in stratification signals the start of the replenishment of nitrate to the surface layers in September and October. The maximum envelope around the mean for nitrate shows some summer events well above the detectable limit (1–2 μM) in June, July and August. Similar events have been attributed by Rees *et al* (Rees *et al.*, 2009) to strong riverine inputs by the River Tamar.

The L4 time-series for nitrite shows subtly different behaviour to that of nitrate. A pre-spring bloom maximum of 0.25 μM is measured in March, which, as with nitrate, declines to below the detectable limit until July. A strong peak in October (which is observed throughout the data set, shown in the maximum and minimum envelope) is possibly attributable to enhanced nitrification of remineralized nitrogen following the breakdown of the late summer blooms which characterize this environment and subsequent mixing of the resultant high NO_2 bottom water following the breakdown of stratification.

Phosphate typically lags nitrate by around 1–2 months at both L4 and E1, the minimum being observed in July (<0.05 μM) and maximum in February (0.55 μM) at L4. This possibly suggests that phytoplankton that can survive nitrate limitation but can thrive on phosphate, can gain the upper hand within the chain of succession for the period between May and August. The presence of phosphate in the absence of detectable nitrate during May–August suggests that the phytoplankton at L4 are predominantly nitrogen limited. Nevertheless, episodic fluvial inputs of high nitrate water from the River Tamar have been shown to temporally alleviate nitrogen limitation (Rees *et al.*, 2009). There is a possible disconnect between the waters at E1 and L4 in the summer months, with E1 consistently reporting higher values (+0.05 μM) in July and August.

Hydes *et al.* (Hydes *et al.*, 2004) report similar values to L4 for winter phosphate on the Malin Shelf (0.53 μM cf. 0.68 μM for the open North Atlantic). The values shown here for E1 are lower than for L4 (0.41 μM cf. 0.55 μM in February). The E1 values are consistent with lower values of inorganic phosphate maxima reported by Southward (Southward, 1980) in relation to the Russell cycle (Russell *et al.*, 1971). Kelly-Gerreyn *et al.* (Kelly-Gerreyn *et al.*, 2007) suggested, when comparing their Ferrybox phosphate concentrations with the 1930–1987 E1 mean winter maximum concentrations, that the English Channel may have returned to the same state as was experienced in the 1960s. Laane *et al.* (Laane *et al.*, 1996), using data from the NOWESP database, show that for the period between 1960 and 1970 the winter maximum phosphate was between 0.3 and 0.5 μM at E1. This contrasts with the periods 1954–1960 and 1970–1985 where the range in winter phosphate was between 0.5 and 0.7 μM. Other stations on the north-west European Shelf such as Port Erin (54° 5′N 4° 46′W) and in the Dutch coastal zone (52°N, 2°E) observe higher winter maxima (>0.7 μM) and greater seasonal variability, although there appears to be no clear relationship between these two stations and E1 in terms of salinity and phosphate concentrations (Laane *et al.*, 1996).

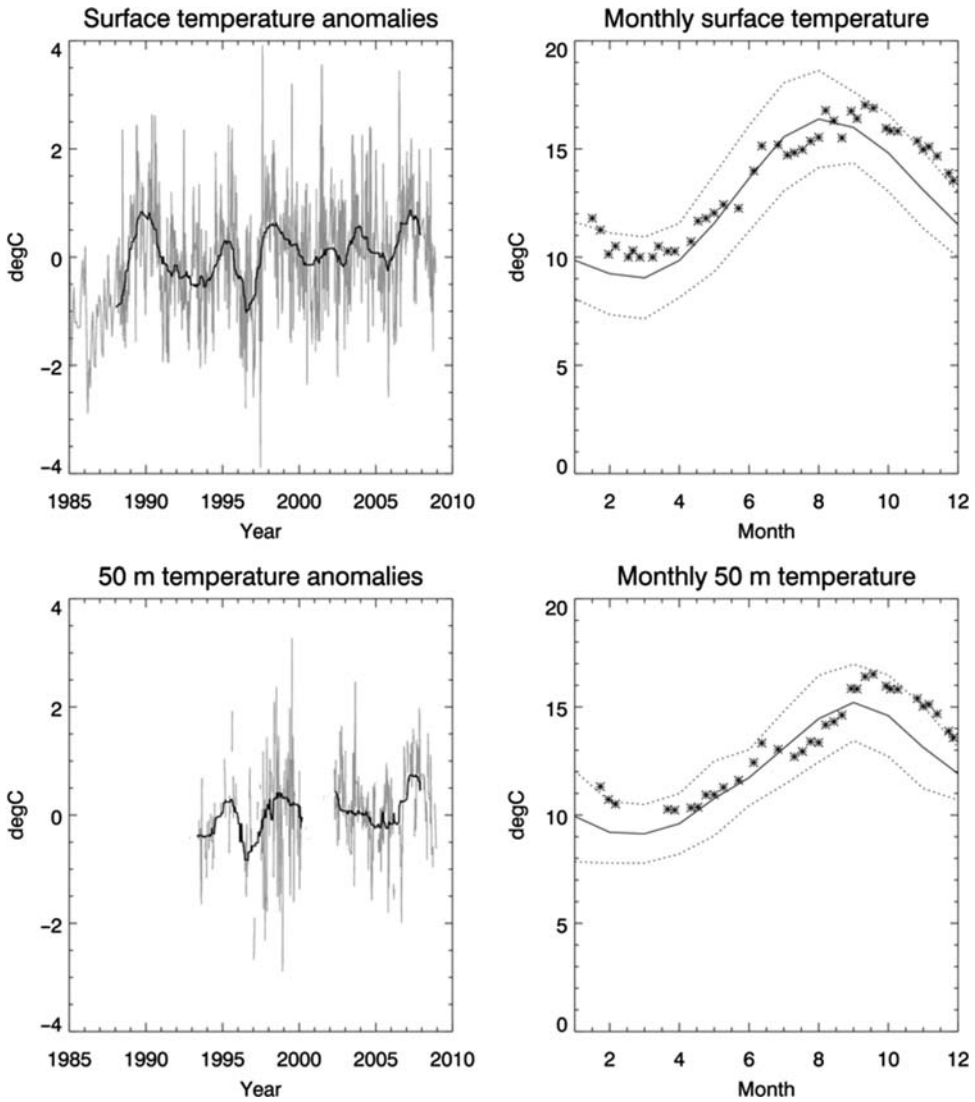

Fig. 8. L4 surface and 50 m temperature time-series analysis. Top panels show the temperature anomalies and monthly averaged temperature for the surface layer (around 2 m) and the corresponding 5-year running median. Bottom panels show the anomalies and averages at 50 m depth. Asterisks represent the data for 2007 and dashed lines the 2σ (2 standard deviations) around the mean during the series. The data between 1987 and 2002 in the upper left panel are monthly averaged satellite SSTs extracted from the Pathfinder data set.

Silicate shows a similar pattern to nitrate, with a maximum in January of around 5 μM and a minimum between May and July at L4. This suggests that a spring bloom, dominated by silicifying diatoms, exhausts the supply of silicon by May. The minimum in silicon, measured in July, marks the likely timing, when it occurs, of the coccolithophore *Emiliana huxleyi*, which can thrive in low silicate conditions (Egge and Aksnes, 1992; Brown and Yoder, 1994). Indeed, this is when they are observed in the Western English Channel (Gordon *et al.*, 2001; Smyth *et al.*, 2002). Interestingly, the values of silicate are much lower in the winter months at E1 with a maximum of 3.5 μM in March. This compares well with the 3.3 μM reported for the Malin Shelf region (Hydes *et al.*, 2004) and lower than the open North Atlantic Ocean values of 4.75 μM. The values at L4 suggest, therefore, that the supply of silicate is likely to come from a different source other than the advection of Atlantic water moving over the continental shelf and along the English Channel (Pingree *et al.*, 1977). The most likely source of silicate is the Tamar estuary.

Chlorophyll

The chlorophyll-*a* time-series (Fig. 12) shows a large degree of annual and interannual variability. At L4, the satellite chlorophyll algorithm is likely to be

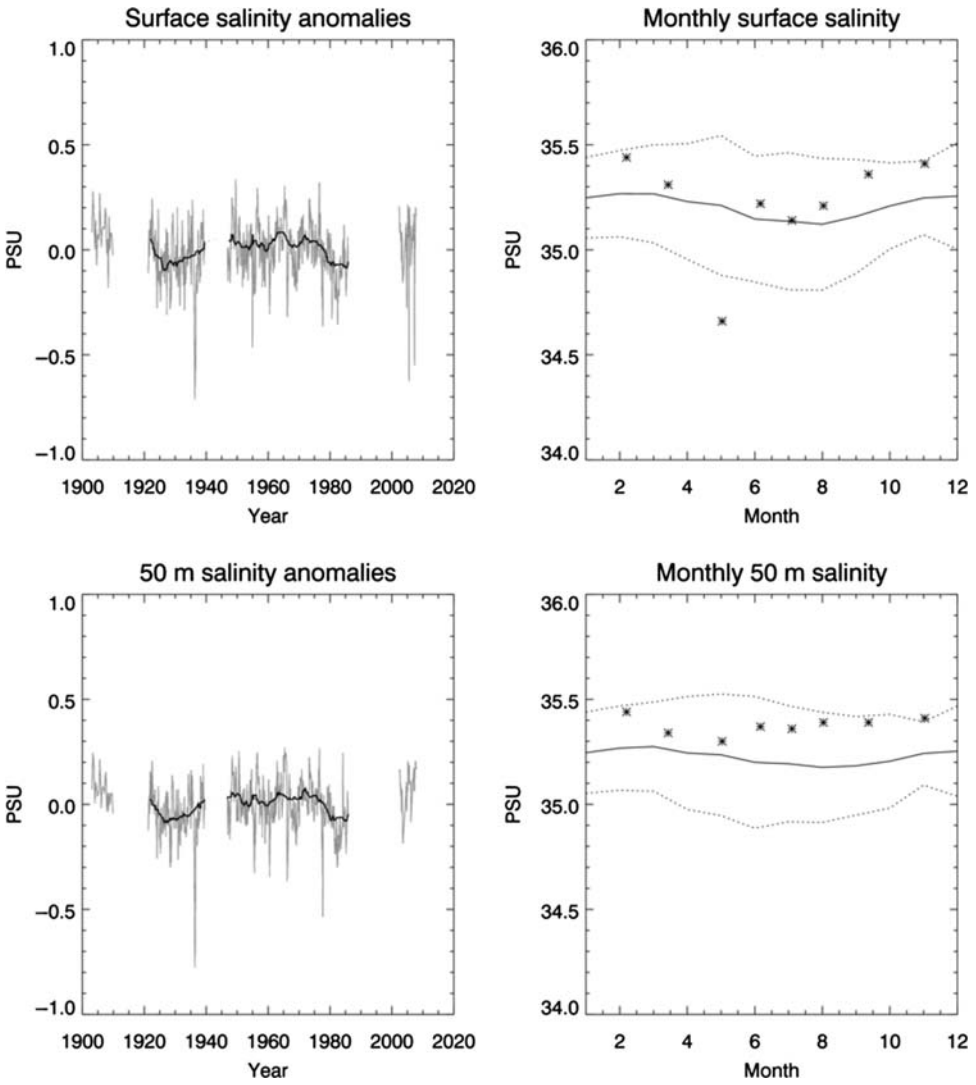

Fig. 9. E1 surface and 50 m salinity time-series analysis. Top panels show the salinity anomalies and monthly averaged salinity for the surface layer (around 2 m) and the corresponding 5-year running median. Bottom panels show the anomalies and averages at 50 m depth. Asterisks represent the data for 2007 and dashed lines the 2σ (2 standard deviations) around the mean during the series.

periodically confounded by the presence of CDOM and suspended particulates (Sathyendranath *et al.*, 1989) and there may also be other coastal effects not accounted for such as adjacency (Santer and Schmechtig, 2000). However, the variability in the satellite chlorophyll signal at L4 is similar to that determined using HPLC and fluorometry, i.e. typically ranging between 0.5 and 2 mg m^{-3} with sharp peaks for short-duration bloom events. Chlorophyll concentrations at E1 seem to be lower than at L4 for most of the year. L4 is affected by two distinct bloom events: the first in May and the second in September, with typical values in the blooms being around 2 mg m^{-3} but may be as high as 8 mg m^{-3} in the autumn bloom. E1 seems to be dominated by a late summer bloom, which is consistent with Fig. 3; E1 being situated on the northern edge of the mid-Channel bloom. The higher concentrations of chlorophyll in the autumn blooms at both stations can be attributed to phytoplankton seasonal succession dynamics. The spring bloom is generally dominated by diatoms, whereas the autumn is characterized by dinoflagellates, such as e.g. *Karenia mikimotoi*. Dinoflagellates (unlike diatoms) are motile (Ryan *et al.*, 2009; Schaeffer *et al.*, 2009) and can therefore access nutrients below the nutricline before swimming back to the surface layer to proliferate in the light. The phytoplankton seasonal succession at L4 and long-term phytoplankton dynamics are discussed by Widdicombe *et al.* (Widdicombe *et al.*, 2010).

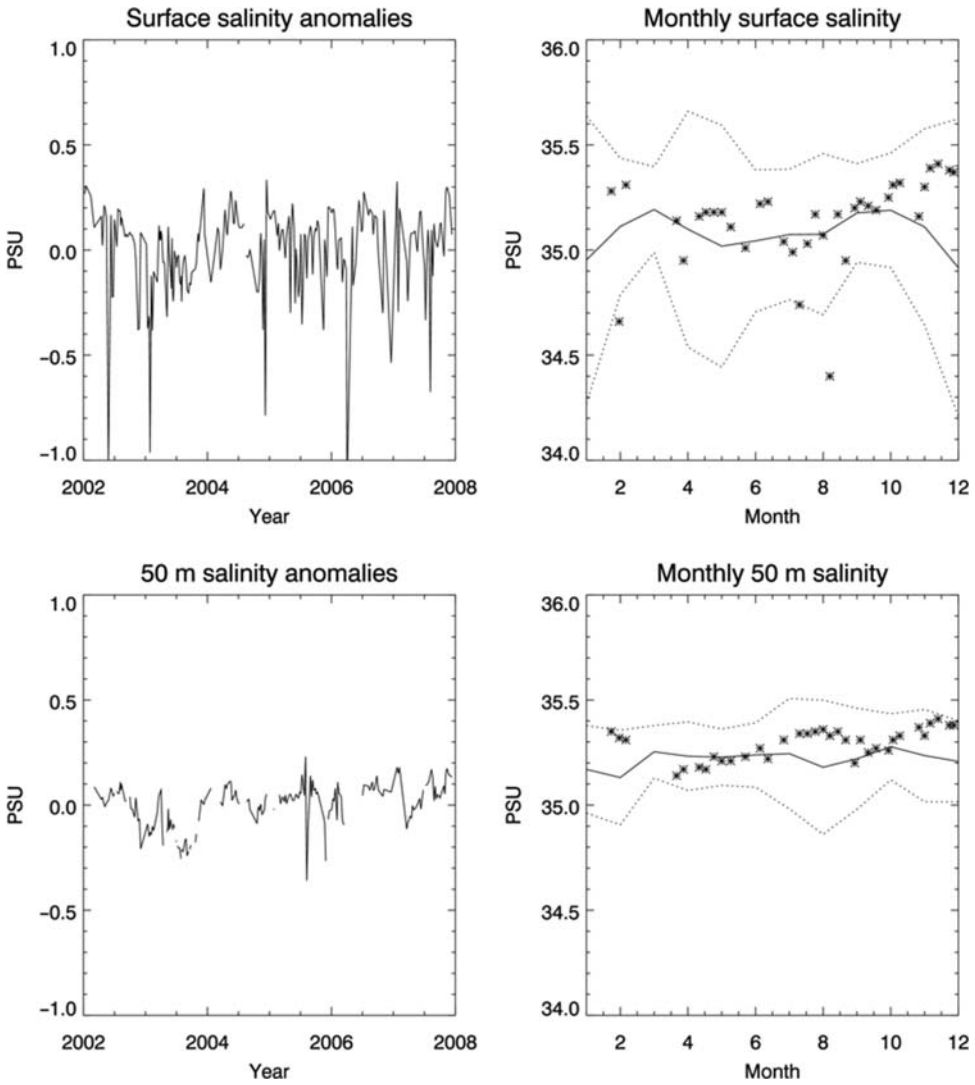

Fig. 10. L4 surface and 50 m salinity time-series analysis. Top panels show the salinity anomalies and monthly averaged salinity for the surface layer (around 2 m) and the corresponding 5-year running median. Bottom panels show the anomalies and averages at 50 m depth. Asterisks represent the data for 2007 and dashed lines the 2σ (2 standard deviations) around the mean during the series.

DISCUSSION

The sea surface temperature increases of around 0.6°C per decade over the past 20 years at stations E1 and L4, resulting in temperatures approximately 0.8°C above the long-term average, are consistent with rises reported across the UK shelf seas (MCCIP, 2008). These temperature rises are not confined to the surface only, with the temperature at the bottom of the water column seeing rises of equal magnitude. Interestingly, the period of greatest temperature rise (Fig. 6; during the 1990s) coincided with a corresponding reduction in the long-term running median surface wind speed (Fig. 4) from 3.5 to 2.75 ms^{-1} and an increase in the surface solar irradiation by around 20% (Fig. 5). Both the surface zonal wind strength (the westerly vector wind) and PAR were correlated (with the opposite sign) to the larger scale forcing of the NAO. A reduction in the wind speed, and hence the wind stress (proportional to the square of the wind speed), and an increase in the surface irradiance would both act to strengthen stratification and enhance the warming of the top mixed layer of the water column. This explains the warming during the stratified phase of the year. During the winter period, the sea-surface temperature is related to air temperature and more likely to be directly influenced by large-scale synoptic processes such as the NAO. The net heat flux anomaly calculations (Fig. 7) possibly help quantify this assertion of increasing irradiance and reduction in wind speed serving to cause the recent

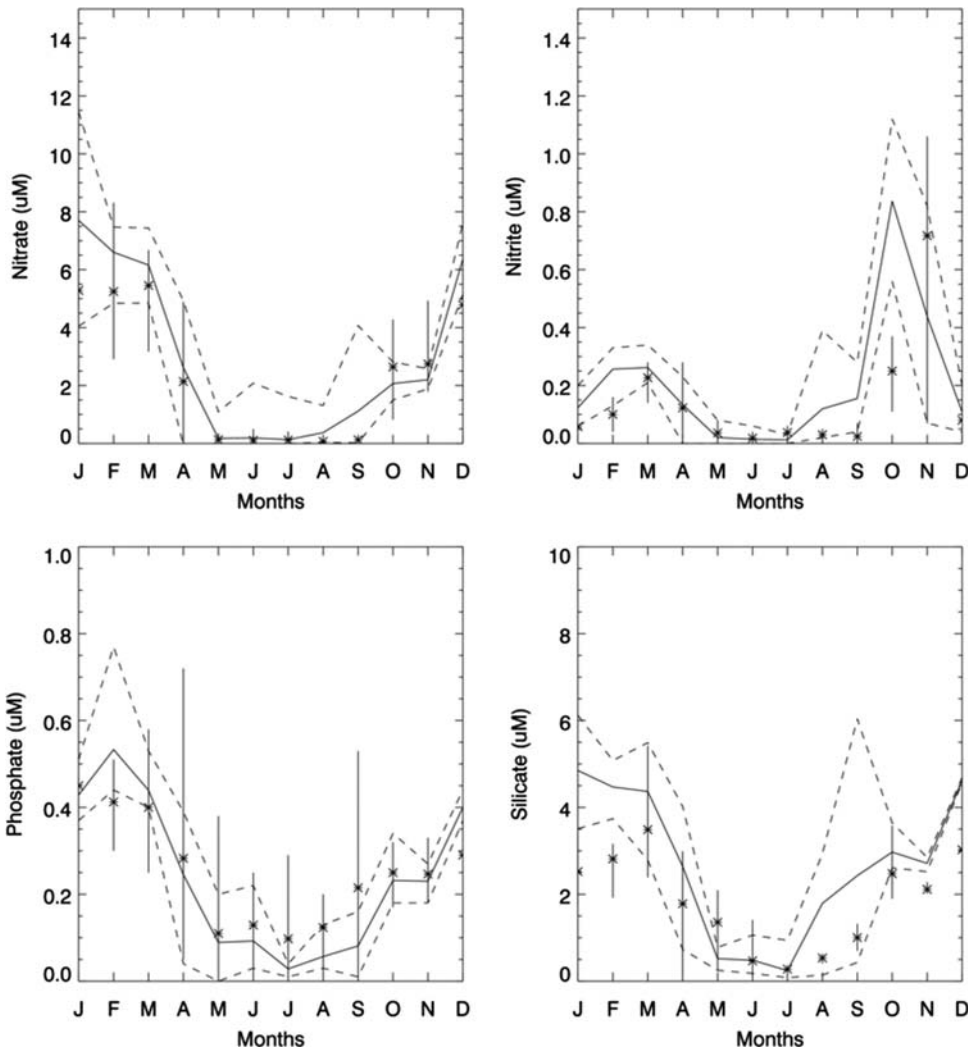

Fig. 11. L4 and E1 monthly averaged surface nutrient concentrations for nitrate, nitrite, phosphate and silicate over the period 2004–2008. The solid line represents the average for the month, the dashed lines either side the maximum and minimum recorded for L4. E1 nutrient data are represented as asterisks with the bars showing the maximum and minimum range for a given month.

warming trend. However, without fine temporal resolution measurements quantifying each component of the heat budget, bulk formulations will always fall prey to being functions of the forcing parameters against which relationships are sought. This being said the correlation between irradiance and the net heat flux anomaly is 0.87 (explaining 75% of the variance) and the correlation between wind speed and the net heat flux anomaly is −0.52 (explaining 27% of the variance).

The temperature changes reported at E1 are consistent with those of other long-term series on the north-west European Shelf. The Malin Head coastal station (55° 23′N, 7° 23′W), where records began in 1960, also shows an increase since the mid-1980s of around 0.6°C per decade. The Helgoland Roads Station (54° 11′N, 7° 54′E) temperature series (1950–present) shows an increase of 1.5°C over the same period as does the Port Erin (54° 05′N, 4° 46′W) series which has a comparable length to the E1 observational period, having begun in 1904.

The nutrient concentrations at E1 are consistent with open-shelf rather than oceanic values (Hydes *et al.*, 2004). This is because the physical processes at the shelf break tend to insulate the Western English Channel from the Atlantic Ocean (Pingree *et al.*, 1999). There is evidence from the difference in nutrient concentrations, that L4 is more directly affected by riverine inputs than E1. The silicate concentrations at E1 are consistent with open-shelf values and the timings of the maximum in March (3.5 μM; Fig. 11) with the maximum in salinity (35.26; Fig. 9) suggests a source other than Atlantic water (Pingree *et al.*, 1977). The variability in the summer month values of nitrate and phosphate (Fig. 11) at L4, which is simply

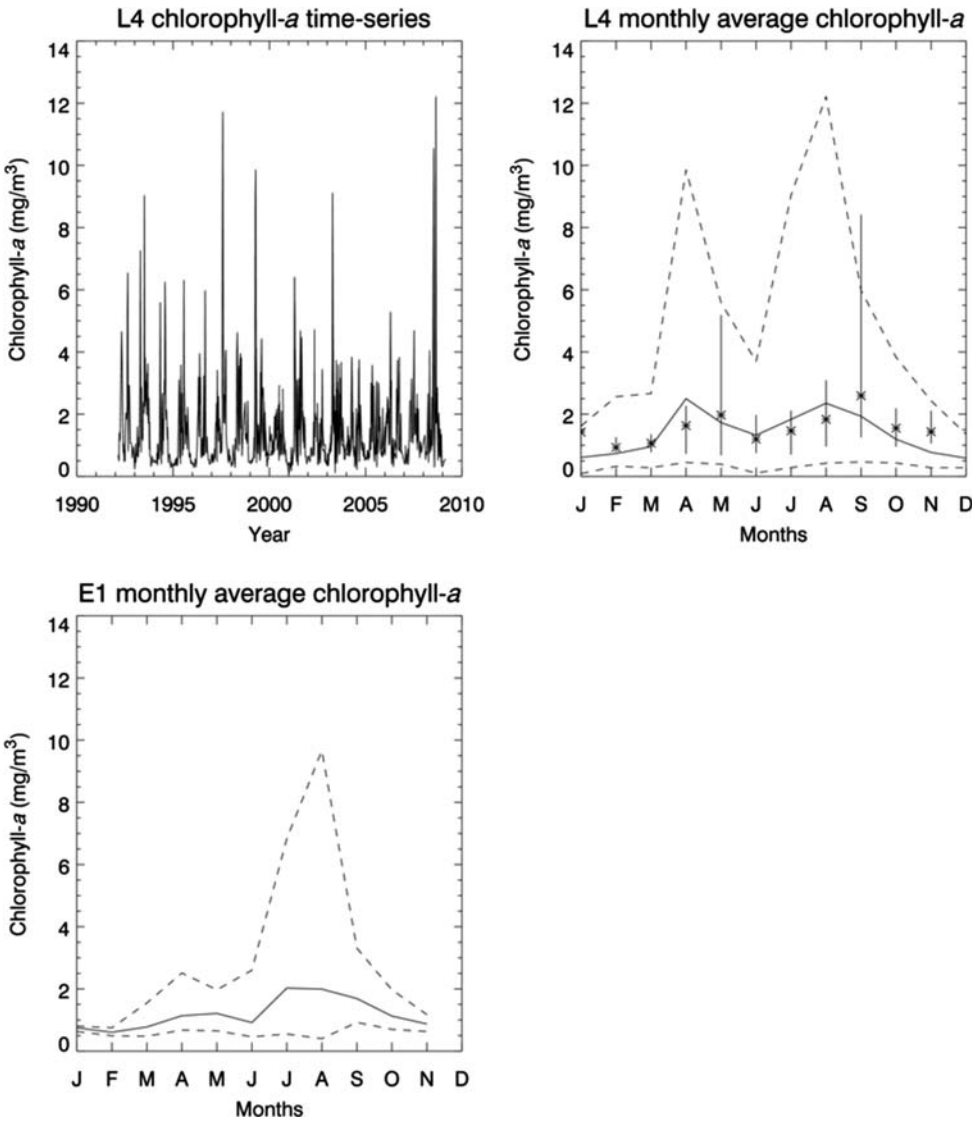

Fig. 12. Top left panel: L4 chlorophyll-*a* time-series (1992–2008) using a combination of HPLC and fluorometric methods. Top right panel: solid line shows the mean monthly averaged chlorophyll-*a* at L4 with the maximum and minimum envelope of values showed as the dashed line. Satellite derived chlorophyll-*a* and associated range (period 1998–2005) are given by the asterisks and bars, respectively. Lower left panel shows the mean monthly and range of chlorophyll-*a*, derived using satellite data at E1.

not reproduced at E1, shows a strong linkage to the Tamar estuary as reported elsewhere (Rees *et al.*, 2009). It may be concluded that the nutrient concentrations at E1 are subject to larger scale climatic drivers, such as the NAO and Russell cycle, and L4 is subject to the variability of land-sea exchanges via the Tamar estuary superimposed on background climatologies.

The sporadic increases in nutrients at L4, driven by fluvial inputs from the Tamar, are consistent with the large variability in the surface salinity anomalies (Fig. 10). As the variability is not reproduced at 50 m depth, the freshening events are restricted to the surface layer (typically down to 20 m depth), forming surface lenses of fresher water. The introduction of fresher surface water causes changes in buoyancy, and hence turbulence, which are critical in determining phytoplankton growth (Huisman *et al.*, 1999). Indeed, Lewis and Allen (Lewis and Allen, 2009) have already reported that observed changes in phytoplankton community are related to salinity at L4.

ACKNOWLEDGEMENTS

The authors would like to thank the crews of the Plymouth Quest and MBA Sepia for the years of

service they have provided; the British Atmospheric Data Centre for provision of the ECMWF ERA-40 data. The WCO represents SO10 (www.westernchannelobservatory.org.uk). The Marine Environmental Change Network ensured the continuity of the E1 series between 2002 and 2005. Thanks also to Theresa Shammon for providing the Port Erin data.

FUNDING

This work is funded under the UK Natural Environmental Research Council Oceans 2025 program as part of Theme 10, Sustained Observations.

REFERENCES

Aiken, J. (1984) The Undulating Oceanographic Recorder mark-2—a multirole oceanographic sampler for mapping and modeling the biophysical marine environment. *Adv. Chem. Ser.*, **209**, 315–332.

Araujo, J. N., Mackinson, S., Stanford, R. J. *et al.* (2006) Modelling food web interactions, variation in plankton production, and fisheries in the western English Channel ecosystem. *Mar. Ecol. Prog. Ser.*, **309**, 175–187.

Barlow, R. G., Cummings, D. G. and Gibb, S. W. (1997) Improved resolution of mono-and divinyl chlorophylls a and b and zeaxanthin and lutein in phytoplankton extracts using reverse phase C-8 HPLC. *Mar. Ecol. Prog. Ser.*, **161**, 303–307.

Beaugrand, G. (2004) The North Sea regime shift: evidence, causes, mechanisms and consequences. *Prog. Oceanogr.*, **60**, 245–262.

Beaugrand, G. and Reid, P. C. (2003) Long-term changes in phytoplankton, zooplankton and salmon related to climate. *Global Change Biol.*, **9**, 801–817.

Beaugrand, G., Luczak, C. and Edwards, M. (2009) Rapid biogeographical plankton shifts in the North Atlantic Ocean. *Global Change Biol.*, **15**, 1790–1803.

Brewer, P. G. and Riley, J. P. (1965) The automatic determination of nitrate in sea water. *Deep Sea Res.*, **12**, 765–772.

Brown, C. W. and Yoder, J. A. (1994) Coccolithophorid blooms in the global ocean. *J. Geophys. Res.*, **99**, 7467–7482.

Egge, J. K. and Aksnes, D. L. (1992) Silicate as regulating nutrient in phytoplankton competition. *Mar. Ecol. Prog Ser.*, **83**, 281–289.

Fasham, M. J. R., Holligan, P. M. and Pugh, P. R. (1983) The spatial and temporal development of the spring phytoplankton bloom in the Celtic Sea, April 1979. *Prog. Oceanogr.*, **12**, 87–145.

Gordon, H. R., Boynton, G. C., Balch, W. M. *et al.* (2001) Retrieval of coccolithophore calcite concentration from SeaWiFS imagery. *Geophys. Res. Lett.*, **28**, 1587–1590.

Grasshoff, H. (1976) *Methods of Sea Water Analysis.* Verlag chemie, Weiheim, 317 pp.

Gregg, W. W. and Carder, K. L. (1990) A simple spectral solar irradiance model for cloudless maritime atmospheres. *Limnol. Oceanogr.*, **35**, 1657–1675.

Hawkins, S. J., Moore, P. J., Burrows, M. T. *et al.* (2008) Complex interactions in a rapidly changing world: responses of rocky shore communities to recent climate change. *Clim. Res.*, **37**, 123–133.

Hiddink, J. G. and ter Hofstede, R. (2008) Climate induced increases in species richness of marine fishes. *Global Change Biol.*, **14**, 453–460.

Huisman, J., van Oostveen, P. and Weissing, F. J. (1999) Critical depth and critical turbulence: two different mechanisms for the development of phytoplankton blooms. *Limnol. Oceanogr.*, **44**, 1781–1787.

Hydes, D. J., Gowen, R. J., Holliday, N. P. *et al.* (2004) External and internal control of winter concentrations of nutrients (N, P and Si) in north-west European shelf seas. *Estuarine Coastal Shelf Sci.*, **59**, 151–161.

Jeffrey, S. W. and Wright, S. W. (1997) Qualitative and quantitative HPLC analysis of SCOR reference algal cultures. In Jeffrey, S. W., Mantoura, R. F. C. and Wright, S. W. (eds), *Phytoplankton Pigments in Oceanography: Guidelines to Modern Methods.* UNESCO, Paris, 383 pp.

JGOFS. (1994) Protocols for the JGOFS core measurements. In Ducklow, D., Dickson, A. (eds), 210 pp.

Kelly-Gerreyn, B. A., Hydes, D. J., Hartman, M. C. *et al.* (2007) The phosphoric acid leak from the wreck of the MV Ece in the English Channel in 2006: Assessment with a ship of opportunity, an operational ecosystem model and historical data. *Mar. Pollut. Bull.*, **54**, 850–862.

Kirkwood, D. S. (1989)*Simultaneous determination of selected nutrients in sea water.*. ICES, Report No. CM 1989/C:29.

Laane, R. W. P., Southward, A. J., Slinn, D. J. *et al.* (1996) Changes and variability in salinity and dissolved inorganic phosphate in the Irish Sea, English Channel, and Dutch coastal zone. *ICES J. Mar. Sci.*, **53**, 933–944.

Lewis, K. and Allen, J. I. (2009) Validation of a hydrodynamic-ecosystem model simulation with time-series data collected in the western English Channel. *J. Mar. Sys.*, **77**, 296–311.

Llewellyn, C. A., Fishwick, J. R. and Blackford, J. C. (2005) Phytoplankton community assemblage in the English Channel: a comparison using chlorophyll a derived from HPLC-CHEMTAX and carbon derived from microscopy cell counts. *J. Plankton Res.*, **27**, 103–119.

MCCIP. (2008) *Marine Climate Change Impacts Annual Report Card 2007–2008*. Lowestoft.

NAO. (2009) Available online at: http://www.cru.uea.ac.uk/cru/data/nao.htm.

Nicklisch, A., Shatwell, T. and Kohler, J. (2008) Analysis and modelling of the interactive effects of temperature and light on phytoplankton growth and relevance for the spring bloom. *J. Plankton Res.*, **30**, 75–91.

NOAA. (2009) Available online at: ftp://ftp.ngdc.noaa.gov/STP/SOLAR_DATA/SUNSPOT_NUMBERS/MONTHLY.

O'Reilly, J. E., Maritorena, S., Mitchell, B. G. *et al.* (1998) Ocean color chlorophyll algorithms for SeaWiFS. *J. Geophys. Res.*, **103**, 24937–24953.

OceanColorWeb. (2009) SeaWiFS V5.2 chlorophyll dataset. Available online at: http://oceancolor.gsfc.nasa.gov.

Parker, D. E., Folland, C. K. and Jackson, M. (1995) Marine surface temperature: observed variations and data requirements. *Clim. Change*, **31**, 559–600.

Pathfinder. (2009) AVHRR Pathfinder Dataset. Available online at: http://data.nodc.noaa.gov/pathfinder/Version5.0_Climatologies/Monthly/Night/.

Pingree, R. D. (1980) Physical oceanography of the Celtic Sea and the English Channel. In Banner, F. T., Collins, B. and Massie, K. S. (eds), *The Northwest European Shelf Seas: The Sea-bed and the Sea in Motion.* Elsevier, Amsterdam, 638 pp.

Pingree, R. D., Maddock, L. and Butler, E. I. (1977) Influence of biological-activity and physical stability in determining chemical distributions of inorganic-phosphate, silicate and nitrate. *J. Mar. Biol. Assoc. UK*, **57**, 1065–1073.

Pingree, R. D., Pugh, P. R., Holligan, P. M. *et al.* (1975) Summer phytoplankton blooms and red tides along tidal fronts in approaches to English-Channel. *Nature*, **258**, 672–677.

Pingree, R. D., Sinha, B. and Griffiths, C. R. (1999) Seasonality of the European slope current (Goban Spur) and ocean margin exchange. *Cont. Shelf Res.*, **19**, 929–975.

Reed, R. K. (1977) On estimating insolation over the ocean. *J. Phys. Oceanogr.*, **7**, 482–485.

Rees, A. P., Hope, S. B., Widdicombe, C. E. *et al.* (2009) Alkaline phosphatase activity in the western English Channel: elevations induced by high summertime rainfall. *Estuarine Coastal Shelf Sci.* **81**, 569–574.

Russell, F. S., Southward, A. J., Boalch, G. T. *et al.* (1971) Changes in biological conditions in the English Channel off Plymouth during last half century. *Nature*, **234**, 468–470.

Ryan, J. P., Fischer, A. M., Kudela, R. M. *et al.* (2009) Influences of upwelling and downwelling winds on red tide bloom dynamics in Monterey Bay, California. *Cont. Shelf Res.*, **29**, 785–795.

Santer, R. and Schmechtig, C. (2000) Adjacency effects on water surfaces: primary scattering approximation and sensitivity study. *Appl. Opt.*, **39**, 361–375.

Sathyendranath, S., Prieur, L. and Morel, A. (1989) A 3-component model of ocean color and its application to remote-sensing of phytoplankton pigments in Coastal Waters. *Int. J. Remote Sens.*, **10**, 1373–1394.

Schaeffer, B. A., Kamykowski, D., Sinclair, G. *et al.* (2009) Diel vertical migration thresholds of Karenia brevis (Dinophyceae). *Harmful Algae*, **8**, 692–698.

Schluessel, P., Emery, W. J., Grassel, H. *et al.* (1990) On the bulk-skin temperature difference and its impact on satellite remote sensing of sea surface temperature. *J. Geophys. Res.*, **95**, 13341–13356.

Sharples, J., Ross, O. N., Scott, B. E. *et al.* (2006) Inter-annual variability in the timing of stratification and the spring bloom in the North-western North Sea. *Cont. Shelf Res.*, **26**, 733–751.

Simpson, J. H. (1981) The shelf-sea fronts—implications of their existence and behavior. *Phil. Trans. R. Soc. Lond. Ser. A-Math. Phys. Eng Sci.*, **302**, 531–546.

Smyth, T. J., Moore, G. F., Groom, S. B. *et al.* (2002) Optical modeling and measurements of a coccolithophore bloom. *Appl. Opt.*, **41**, 7679–7688.

Sommer, U. and Lengfellner, K. (2008) Climate change and the timing, magnitude, and composition of the phytoplankton spring bloom. *Global Change Biol.*, **14**, 1199–1208.

Southward, A. J. (1960) On changes of sea temperature in the English Channel. *J. Mar. Biol. Assoc. UK*, **42**, 275–375.

Southward, A. J. (1980) The western English-Channel—an inconstant ecosystem. *Nature*, **285**, 361–366.

Southward, A. J., Butler, E. I. and Pennycuick, L. (1975) Recent cyclic changes in climate and in abundance of marine life. *Nature*, **253**, 714–717.

Southward, A. J., Langmead, O., Hardman-Mountford, N. J. *et al.* (2005) Long-term oceanographic and ecological research in the western English Channel. *Adv. Mar. Biol.*, **47**, 1–105.

UKCP09. (2009) Available online at: http://ukcp09.defra.gov.uk/.

Vargas, M., Brown, C. W. and Sapiano, M. R. P. (2009) Phenology of marine phytoplankton from satellite ocean color measurements. *Geophys. Res. Lett.*, **36**, 5.

WHSC (2009) Available online at: http://woodshole.er.usgs.gov/operations/sea-mat/index.html (accessed 23 October 2009).

Widdicombe, C. E., Eloire, D., Harbour, D. *et al.* (2010) Long-term phytoplankton community dynamics in the Western English Channel. *J. Plankton Res.*, **32**, 643–655.

Wiltshire, K. H. and Manly, B. F. J. (2004) The warming trend at Helgoland Roads, North Sea: Phytoplankton response. *Helgoland Mar. Res.*, **58**, 269–273.

Woodward, E. M. S. and Rees, A. P. (2002) Nutrient distributions in an anticyclonic eddy in the North East Atlantic Ocean, with reference to nanomolar ammonium concentrations. *Deep Sea Res. II*, **48**, 775–794.

Zacherl, D., Gaines, S. D. and Lonhart, S. I. (2003) The limits to biogeographical distributions: insights from the northward range extension of the marine snail, *Kelletia kelletii* (Forbes, 1852). *J. Biogeogr.*, **30**, 913–924.

Zhang, J. Z. and Chi, J. (2002) Automoted analysis of nanomolar concentrations of phosphate in natural waters with liquid waveguide. *Environ. Sci. Technol.*, **36**, 1048–1053.